Green Chemistry

Utilizing Hydrogen Underpotential Deposition in CO Reduction for Highly Selective Formaldehyde Production under Ambient Condition

Journal:	*Green Chemistry*
Manuscript ID	GC-ART-04-2020-001412.R1
Article Type:	Paper
Date Submitted by the Author:	18-Jun-2020
Complete List of Authors:	Yao, Libo; University of Akron, Department of Chemical and Biomolecular Engineering Pan, Yanbo; University of Akron, Department of Chemical and Biomolecular Engineering Shen, Xiaochen; University of Akron, Department of Chemical and Biomolecular Engineering Wu, Dezhen; University of Akron Polymer Engineering Bentalib, Abdulaziz; University of Akron, Department of Chemical and Biomolecular Engineering Peng, Zhenmeng; University of Akron, Department of Chemical and Biomolecular Engineering

ARTICLE

Utilizing Hydrogen Underpotential Deposition in CO Reduction for Highly Selective Formaldehyde Production under Ambient Condition

Received 00th January 20xx,
Accepted 00th January 20xx

DOI: 10.1039/x0xx00000x

Libo Yao,[†] Yanbo Pan,[†] Xiaochen Shen, Dezhen Wu, Abdulaziz Bentalib and Zhenmeng Peng [a]*

Formaldehyde is an essential building block for hundreds of chemicals and a promising liquid organic hydrogen carrier (LOHC), yet its indirect energy-intensive synthesis process prohibits it from playing more significant role. Here we report a direct CO reduction to formaldehyde (CORTF) process that utilizes hydrogen underpotential deposition to overcome thermodynamic barrier and scaling relationship restriction. This is the first time that this reaction is realized under ambient condition. Using molybdenum phosphide as catalyst, formaldehyde can be produced with nearly 100% Faradaic efficiency in aqueous KOH solution, with its formation rate being one order of magnitude higher compared with state-of-the-art thermal catalysis approach. Simultaneous tuning of current density and reaction temperature leads to more selective and productive formaldehyde synthesis, indicating electrochemical and thermal duality of this reaction. DFT calculations reveal that desorption of $*H_2CO$ intermediate likely serves as rate-limiting step, and the participation of H_2O turns the reaction into thermodynamically favorable. Furthermore, a full-cell reaction set-up was demonstrated with CO hydrogenation to HCHO being achieved without any energy input, which fully realizes the spontaneous potential of the reaction. Our study shows the feasibility of combination of thermal and electrochemical approach in realizing thermodynamics and scaling relationship confined reaction, which could serve as a new strategy in future reaction design.

INTRODUCTION

The thriving of hydrogen economy and fuel cell technologies have stimulated extensive research efforts in the associated fields,[1] among which hydrogen storage remains a challenging topic.[2-6] With a hydrogen storage capacity of 8.3 wt.% in its hydrated form, formaldehyde (HCHO) holds a theoretical promise as an excellent liquid organic hydrogen carrier (LOHC) that releases H_2 via decomposition and can be regenerated via hydrogenation.[7-8] It is also advantageous, comparing to other LOHC candidates like methanol and formic acid,[9-11] in terms of its more favorable reaction thermodynamics.[12] However, HCHO was the least investigated among the three chemicals for LOHC application in previous studies, which suffered from the harsh reaction conditions required for HCHO synthesis that caused high energy cost.[13-15] In practice, HCHO is produced by methanol as precursor following the so-called Formox process,[16] which partially oxidizes methanol to HCHO above 400 °C.[17] Considering that methanol is typically synthesized from syngas at elevated temperature and high pressure,[18] the overall HCHO production process is highly energy-consuming which restricts its use for LOHC application. Besides, HCHO is an important precursor for synthesizing many more complex chemicals, like resins, 1,4-butanediol, polyols and so on, which demands annual HCHO production of over 50 million tons.[19-21] New, cost-effective method for HCHO synthesis would not only decrease the production cost for its many uses but also enable its application as LOHC for hydrogen storage research.

From thermodynamic point of view, gaseous HCHO can be directly synthesized from syngas via CO hydrogenation, which would skip the energy intensive methanol synthesis and the Formox steps. The reaction has a positive ΔG_0 value in gas phase (Eq. 1), making it barely possible to take place under standard condition.[22] However, the ΔG_0 would turn slightly negative when the reaction occurs in an aqueous phase (Eq. 2), benefiting from the contribution of heat released during HCHO solvation. This offers an opportunity to realize aqueous HCHO synthesis from direct CO hydrogenation.[11]

$$CO_{(g)} + H_{2(g)} \rightarrow HCHO_{(g)} \quad \Delta G^0 = +34.6\ kJ/mol \qquad (1)$$

$$CO_{(g)} + H_{2(g)} + H_2O_{(aq)} \rightarrow HCHO \cdot H_2O_{(aq)} \quad \Delta G^0 = -7.1\ kJ/mol \qquad (2)$$

As a matter of fact, Tanksale et al. demonstrated success by thermally catalyzing CO hydrogenation using Pd-Ni and Ru-Ni/Al_2O_3 catalysts in aqueous solution,[22-23] with a small amount of HCHO being obtained that proved the viability of this route. However, the achieved HCHO generation rate was low, being less than 3 mg/(g_{cat} h) even using the best performed catalyst and under a harsh condition of high pressure (20-120 bars), which is far from being satisfactory in terms of potential industrial application. The slow reaction kinetics can be explained under scope of the discovered scaling relationship in catalysis.[24-26] CO molecules chemisorb more strongly to catalyst

[a] Department of Chemical and Biomolecular Engineering, The University of Akron, Akron, OH 44325, United States.
[†] These authors contributed equally to this article.
* Correspondence author: zpeng@uakron.edu.

than H_2 does in a generic trend. This leads to the active sites being dominantly occupied by CO with few active sites available for H_2 molecules to adsorb and dissociate, which consequently inhibits the reaction. From this perspective, it would be challenging to realize efficient CO hydrogenation to aqueous HCHO, unless there are means to break the scaling relationship to achieve more balanced H_2 adsorption.

Electrocatalysis has received significant attention in reducing CO_2 to energy fuels in aqueous phase under mild condition. In comparison, CO electrochemical reduction was less intensively investigated.[27-29] Instead, more research focus was put on the tandem reaction starting from CO_2, with the aim to establish a CO_2-CO-chemical network.[30-32] Similar to CO_2 electrochemical reduction, Cu-based materials were mainly used in CO electrochemical reduction, that led to generation of different products including methane,[30,33] hydrocarbons,[34,35] alcohols[29,36] and acetates.[37-39] To the best of our knowledge, no direct HCHO synthesis via CO electrochemical reduction has been achieved, which indicates that the catalysis mechanism of Cu-based materials doesn't favor HCHO formation. New catalysis mechanism would be required to realize electrochemical synthesis of aqueous HCHO.

Herein, we report a new synthesis strategy that combines thermal CO reduction catalysis with hydrogen underpotential deposition, which is a pre-step for hydrogen evolution reaction (HER), to reduce CO to aqueous HCHO. Direct, selective CO reduction to formaldehyde (CORTF) is achieved under ambient condition using molybdenum phosphide (MoP) catalyst, which has been previously studied as an efficient catalyst in hydrogen evolution reaction (HER) but has poor CO adsorption capability.[40] We report that formaldehyde can be generated with 100% selectivity at room temperature via combinational utilization of electrochemical and thermal reaction mechanisms. The CORTF process improves formaldehyde formation rate to one order of magnitude higher than the previous thermal catalysis method.[22-23] We further demonstrate a spontaneous, selective HCHO synthesis at room temperature in a full cell, with CO fed to one electrode for CORTF and H_2 fed to the other for hydrogen oxidation reaction. Effective aqueous HCHO production is realized without any energy input, confirming a great potential of this new CORTF method.

EXPERIMENTAL

Catalyst Preparation.

Molybdenum phosphide (MoP) was prepared by a temperature programmed reduction (TPR) method.[41] The molybdenum precursor, ammonium molybdate tetrahydrate, $(NH_4)_6Mo_7O_{24}{\cdot}4H_2O$, and the phosphorus source, ammonium phosphate dibasic, $(NH_4)_2HPO_4$, were dissolved in DI water equimolarly in terms of Mo and P. The mixture was stirred and dried overnight at 80 °C, followed by calcination at 500 °C for 4 h. The resultant sample then underwent TPR with flowing H_2 (50 ml/min). The procedures included ramping to 350 °C at a rate of 5 °C/min, followed by increasing to 650 °C at 2 °C/min and holding at this temperature for 2 h. The sample was cooled down to room temperature and purged with Ar for another 1h before being collected.

Catalyst Characterization.

The as-prepared and spent MoP samples were characterized by Transmission Electron Microscopy (TEM) using a JEOL JEM-1230 microscope with an accelerating voltage of 120 kV. High-resolution TEM (HRTEM) images were taken using a FEI Tecnai G2 F20 microscope operated at 200 kV. The powder X-Ray diffraction (PXRD) patterns were recorded on a Rigaku Ultima IV multipurpose X-ray diffraction system with CuKα radiation source. The XPS spectra were obtained with PHI 5000 Versaprobe II X-Ray Photoelectron Spectrometer. SEM image and EDX mapping were obtained on a Tescan LYRA3 machine with a working voltage of 10 kV for SEM and 20 kV for the mapping mode. In situ diffuse reflectance infrared Fourier transform spectroscopy (DRIFTS) experiments were conducted with a Nicolet 6700 FTIR spectrometer equipped with Harrick Praying Mantis DRIFTS accessory. The spectra were recorded by collecting 64 scans at a resolution of 4 cm^{-1}.

Electrode Preparation and Electrochemical Measurements.

The electrochemical measurements were conducted by a Gamry Reference 600+ potentiostat in an undivided electrochemical cell which includes a 3-electrode configuration. MoP deposited on carbon cloth (MoP/CC) was used as working electrode (WE), Ag/AgCl and Pt wire were used as reference electrode (RE) and counter electrode (CE), respectively. For the preparation of WE, MoP ink was first made by dispersing 1 mg MoP powder in 0.5 mL isopropanol which contains 2 µL Nafion as binding agent. After sonification, the ink was uniformly dispersed on a 2 cm × 1 cm hydrophilic carbon cloth. In most experiments, 0.5 M KOH was used as default electrolyte unless otherwise noted. All potentials in this work were converted to those in the scale of reversible hydrogen electrode (RHE) by calibration, in 0.5 M KOH the transformation is shown in eq. 3:

$$\boldsymbol{E(RHE) = E(Ag/AgCl) + 0.906} \qquad (\mathbf{3})$$

Polarization curves were obtained under linear sweep voltammetry with 10 mV/s scan rate. Electrochemical impedance spectroscopy (EIS) was carried out in the frequency range of 100000 to 0.01 Hz under the amplitude of 10 mV.

The half-cell CO electrochemical reduction test was performed with continuous feeding of CO gas. Prior to each run, CO was bubbled to the solution for 1 h with the flow rate of 20 ml/min for saturation, and it was continuously fed at the same rate during the measurement.

The full-cell CO reduction was conducted in a H-type 2-compartment cell with a 2-electrode configuration in 0.5 M KOH electrolyte. A FUMASEP-FAB-130 anion exchange membrane was placed between the two compartments. The MoP/CC electrode was placed in cathodic compartment with 20 ml/min CO feed, while the Pt electrode was placed in the annodic one with 20 ml/min H_2 being continuously flowed. The cathodic, anodic and overall reactions are shown in the following:

$$\boldsymbol{Cathode}: \ \boldsymbol{CO + 3H_2O + 2e^- \rightarrow HCHO \cdot H_2O + 2OH^-} \qquad (\mathbf{4})$$

$$Anode: H_2 + 2OH^- \rightarrow 2H_2O + 2e^- \quad (5)$$

$$Overall: CO + H_2 + H_2O \rightarrow HCHO \cdot H_2O \quad (6)$$

Product Analysis and Quantification.

Gas products of the reaction were analyzed through an Agilent 6890 GC-MSD, and liquid products were analyzed by ^{1}H-NMR using a Bruker AVIII 750 MHz NMR spectrometer. Typically, 500 µL of collected electrolyte after reaction was mixed with 100 µL D_2O. The ^{1}H spectrum was measured with water suppression using a pre-saturation method. As the spectra from the GC-MS and ^{1}H-NMR (**Figure S1 and S2**) have shown, no carbonaceous gaseous products or liquid products other than formaldehyde have been detected under our reaction condition (50 µA cm^{-2}). Therefore, the products can be considered as to include only H_2 and HCHO, and the calculation of Faradaic efficiency (FE) can be performed based on formaldehyde formation. Formaldehyde is quantified by an adapted acetylacetone method.[42] To start with, 0.25% (v/v) acetylacetone solution was prepared by dissolving 25 g ammonium acetate, 3 ml acetic acid and 0.25 ml acetylacetone in DI water and fix the volume of solution to be 100 ml. Then a series of formaldehyde standard solutions (0, 0.083, 0.333, 0.833, 1.667, 2.5 and 2.917 µg/ml) were prepared. Next, mix each of 5 ml standard solution with 1 ml 0.25% acetylacetone solution and put in boiling water bath for 3 min. After cooled down to room temperature, the solution was transferred to Shimadzu UV-2600 spectrophotometer for the detection of absorbance from 800-190 nm wavelength. A working curve (**Figure S4**) was constructed by building the relationship between the absorbance at 413 nm (**Figure S3**) and concentration for standard solutions, and it turned out to be perfectly linear. The curve was therefore used for the quantification of formaldehyde for all the samples obtained in this work. The Faradaic efficiency of HCHO (FE_{HCHO}) and can be calculated using $FE_{HCHO} = (nFxV)/(I \times t) \times 100$, where n is the number of electrons being transferred, F is Faraday's constant, x is the concentration of HCHO, V is the volume of electrolyte, I is the current and t is the reaction time.

DFT Calculations.

DFT calculations were performed using the Quantum ESPRESSO package.[43] Generalized gradient approximation (GGA) and the Perdew-Burke-Ernzerhof (PBE) with projector-augmented wave (PAW) sets from PSlibrary 0.3.1 were used to carry out the structure relaxation and energy calculation.[44] The bulk lattice of MoP was optimized prior to the cleavage of the (001) surface. The slab model of MoP was constructed using a p (3 × 3) unit cell with six layers of close-packed (001) surfaces which were separated by a vacuum layer of 20 Å in the direction perpendicular to the surface. A plane wave basis set was used with a cutoff energy of 450 eV with the density cutoff being 4500 eV and a Monkhorst-Pack k-point mesh being 5 × 5 × 1, and the Fermi-level smearing was set at 0.1 eV. The bottom four layers of atoms were held fixed in their bulk positions, while the top two layers of atoms and all adsorbate degrees of freedom were allowed to relax.

RESULTS AND DISCUSSIONS

Characterization of MoP Catalyst.

The MoP synthesis follows a widely adopted temperature programmed reduction method in previous studies.[41] The XRD pattern indicates a pure hexagonal structure (ICDD 03-065-6487) with a space group belonging to $P\bar{6}m2$ (**Figure S5**). HRTEM characterization exhibits well-arrayed (001) and (101) planes with d-spacing of 0.32 and 0.21 nm, respectively (**Figure S6a**). A thin amorphous layer is observable on MoP surface, which suggests slight surface oxidation caused by sample exposure to atmosphere.[45] SEM imaging and EDX mapping show an even distribution of Mo and P elements throughout the sample (**Figure S6b-d**), which was in consistence with the XRD data and confirmed a uniform MoP phase. XPS spectroscopy of Mo 3d and P 2p bands show dominant signals assignable to MoP phase (**Figure S7**). The Mo 3d spectra exhibit two minor deconvoluted peaks at 231.4 and 234.3 eV, which are assignable to Mo^{6+} as a result of slight surface oxidation due to exposure to air, which is in good agreement with previous reports.

Experimental Evaluation of CO Reduction to Formaldehyde.

The first step in achieving CO reduction to formaldehyde (CORTF) would be finding an appropriate electrolyte. **Figure 1a** shows the linear sweep voltammetry (LSV) curves of MoP in CO-saturated acidic (0.5 M H_2SO_4, pH=0.6), neutral (0.5 M Na_2SO_4, pH=6.7), and alkaline (0.5 M KOH, pH=13.2) media. The currents were corrected with the ohmic resistance (Rs, **Table S1**) which were fitted with equivalent circuit obtained from electrochemical impedance spectroscopy (**Figure S9**). For comparison purpose, LSV curves were also obtained under CO absence condition, which corresponded to HER (**Figure S10**). In both cases, the catalytic activity of MoP represented by current density follows a same order of H_2SO_4>KOH>>Na_2SO_4. Tafel plots were subsequently derived from the LSV curves (**Figure S11**). Nearly identical values and Tafel slopes, 92.0 mV dec^{-1} in presence of CO versus 93.5 mV dec^{-1} in absence of CO, were obtained in H_2SO_4, suggesting the activity accounts predominantly for HER but little CO reduction. Interestingly in KOH electrolyte, the Tafel slope changed significantly from 94.4 to 119.3 mV dec^{-1} after CO was introduced, suggesting an alteration in reaction kinetics in presence of CO and implying possible CORTF occurrence. Similar phenomenon was also observed in neutral electrolyte, however the overall activity was too low to be considered. The CORTF reaction was confirmed by analyzing the liquid and gas products collected at -5 mA cm^{-2} with GC-MS and ^{1}H-NMR (**Figure S1 and S2**), which found HCHO as the only product besides H_2. Quantitative analyses show little HCHO being produced in acidic electrolyte but considerable HCHO formation in alkaline solution (Figure 1b). The finding indicates HCHO could indeed be produced via CORTF in appropriate electrolyte even under ambient condition. It needs noted that HCHO Faradaic efficiency (FE_{HCHO}) was calculated to be only 0.52% under the specific testing condition, suggesting a need for performance optimization.

By carefully comparing with the LSV curve obtained in Ar-protected 0.5 M KOH, we observed the current density was lower below about -0.2 V but higher above this potential when CO was present (**Figure 1c**). It revealed the CORTF contribution

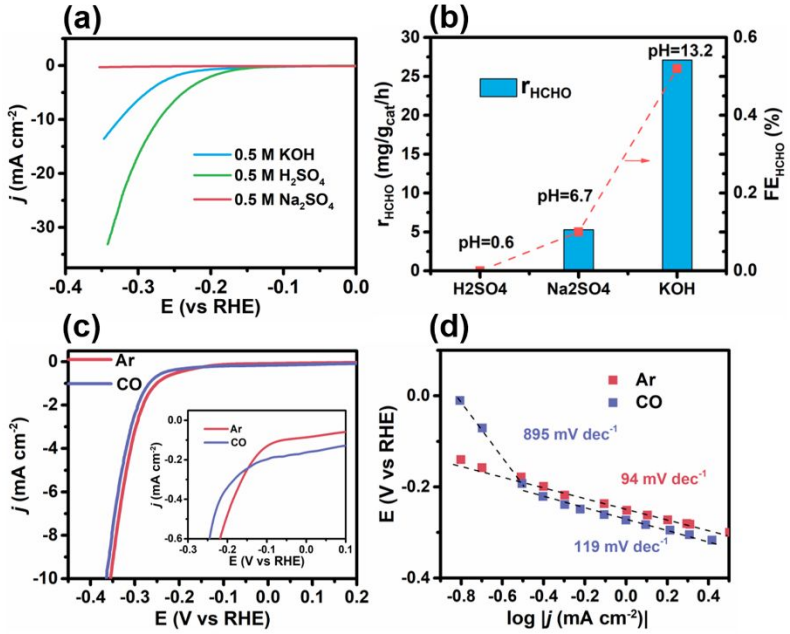

Figure 1. Electrocatalytic properties of MoP with and without CO presence. (a) Polarization curves in CO-saturated acidic (0.5 M H_2SO_4, pH=0.6), neutral (0.5 M Na_2SO_4, pH=6.7) and alkaline (0.5 M KOH, pH=13.2) electrolytes. (b) Effect of electrolyte on formaldehyde formation at -5 mA cm^{-2}. (c) Comparison of the polarization curves and the zoom-in curves from -0.2 to 0.1 V (inset) in 0.5 M KOH electrolyte with and without CO. (d) Tafel plots obtained from polarization curves in c.

to the overall current density is more significant before the onset potential, where the hydrogen underpotential deposition (HUPD) occurs. This is a good indication that the deposited hydrogen is combined with CO for formaldehyde production. **Figure 1d** shows the difference between the two Tafel plots to yield more insights. The Tafel plot with CO shows two linear sections, which intersected at about -0.2 V in potential and about -0.5 in log |j| that corresponds to a low current density of -0.3 mA cm^{-2}. The plot exhibits an abnormally high Tafel slope of 895 mV dec^{-1} in the upper potential range, i.e., the lower current density range. This value is distinct from 119 mV dec^{-1} in the lower potential range where HER dominates, implying possible dominance by the CORTF reaction in its regime.

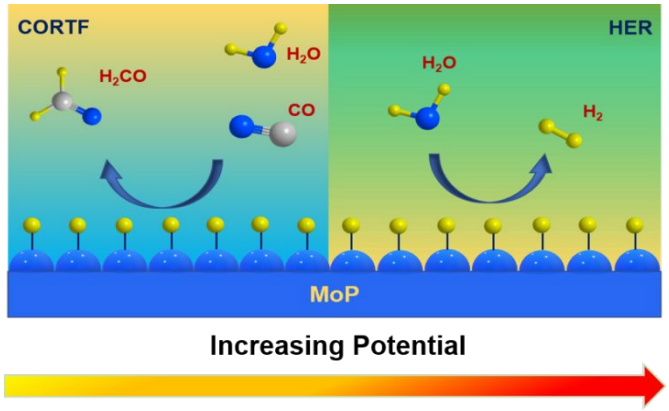

Figure 2. Schematic representation of competitive CORTF and HER pathways.

As shown in our in situ DRIFTS experiment (**Figure S12**) as well as in previous studies,[41] it is known that MoP barely chemisorbs CO. CORTF is likely resulted from reaction between dissolved CO and in situ generated *H species on MoP active sites. In other words, there would exist a competition relationship between CORTF and HER (**Figure 2**). Sharing a same hydrogen deposition step that generates *H species, the preference of product is dependent on potential, as higher overpotential explicitly triggers HER, while CORTF is more significant within underpotential range (<-0.2 V). The HCHO generation rate (r_{HCHO}) and FE_{HCHO} as well as their dependence on the testing condition were thus carefully examined in the lower current density range. There is a clear trend that with a decrease in current density, r_{HCHO} decreases monotonously while FE_{HCHO} keeps increasing (**Figure 3a**), with FE_{HCHO} reaching 96.6% at -5 μA cm^{-2}. The finding reveals that HCHO can be more selectively produced at a lower current density, i.e., at a more positive potential. The alteration in product distribution between HCHO and H_2, considering the HER kinetics is purely potential dependent, implies the CORTF kinetics does not simply rely on the electrochemical potential but also some other factors. This was confirmed by examination of the temperature effect on the reaction kinetics and selectivity by keeping the electrode potential unchanged (E=-30 mV, **Figure 3b**). Both the r_{HCHO} and FE_{HCHO} increase with temperature, suggesting CORTF as a "hybrid" reaction with the kinetics being influenced by not only electrochemical potential but also thermochemistry. An apparent activation energy of 17.1 kJ/mol was determined for CORTF from the Arrhenius plot (**Figure S13**). The temperature effect shows a same trend when the current density was fixed at -250 and -50 μA cm^{-2} (**Figure S14**). The exception appeared at -5 μA cm^{-2}, where both r_{HCHO} and FE_{HCHO} became nearly independent on temperature with FE_{HCHO} approaching 100%. At this low current density, the CORTF rate would

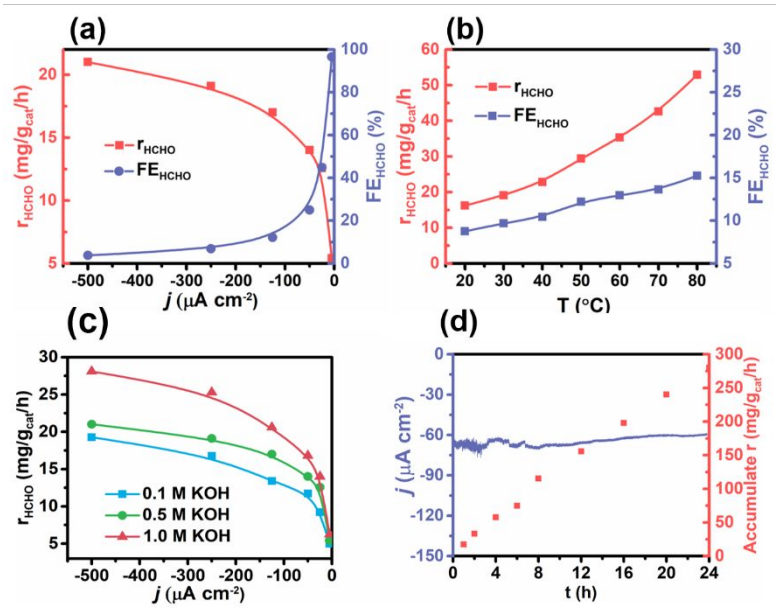

Figure 3. CORTF properties on MoP and the influencing factors. (a) Measured r_{HCHO} and FE_{HCHO} as function of current density. (b) Temperature effect on r_{HCHO} and FE_{HCHO} obtained at E=-30 mV (vs RHE). (c) Effect of electrolyte concentration on r_{HCHO}. (d) Stability test at 0.2 V vs RHE.

likely be restricted by the *H generation rate but not the following steps that are influenced by temperature. By simultaneously tuning the current and temperature, HCHO can be produced at a rate of over 30 mg/(g_{cat} h) with more than 50% Faradaic efficiency (**Figure S14b**). The activity represents over one order of magnitude higher than state-of-the-art thermal catalysis approach (**Table S2**) The electrolyte concentration effect on the CORTF properties was also examined (**Figure 3c** and **Figure S15**). An increase in the KOH concentration led to r_{HCHO} enhancement. It is well known that a higher electrolyte concentration can substantially increase the HER intrinsic activity, leading to more positive onset potential and lower Tafel slope.[46,47] Such enhancement would contribute to more efficient hydrogen deposition and subsequent CO reduction.

The durability test at 0.2 V vs RHE, where CORTF dominates, shows a minor decrease of less than 20 μA cm^{-2} in the current density within 24 h, suggesting a good stability of the MoP catalyst (**Figure 3d**). The slight reaction rate decrease could be related to reduced CO mass transfer efficiency caused by a mismatch between the continuous CO_{aq} consumption and under-compensation due to a low solubility (**Figure S16**). Based on measurement of the accumulative HCHO production amount after different periods of time, it can be deduced that the CORTF reaction rate was relatively faster at the very beginning and then remained steady till completion of the stability test. It is worth mentioning that the measured electrode potential became positive when the current density was below -250 μA cm^{-2} (**Figure S17**), which can be attributed to a more positive CORTF potential than HER induced by CO presence (**Figure S18**). XRD characterizations of the MoP catalyst after the stability test show no observable difference to the fresh sample, confirming its structural stability (**Figure S8**).

Proposed Reaction Pathway and DFT Calculations

Density functional theory (DFT) simulations of both CORTF and HER pathways were conducted to gain more insights into the reaction mechanism and properties (**Figure S19**). **Figure 4** presents the calculated Gibbs free energy diagram for the two reactions on Mo-terminated MoP (001) surface at E=0 V. Detailed structure and energy information of surface intermediates are summarized in **Figure S20** and **Table S3**, respectively. The two reactions share a same initial step (step 1), i.e. the Volmer step, in which *H is generated on MoP surface. The generated *H would follow the Heyrovsky mechanism to further electrochemically react that leads to HER and thus H_2 formation. Alternatively, *H would react with free molecular CO_{aq} to form *HCO (step 2), which involves no electron transfer and is hence a non-galvanic process. *HCO would be further hydrogenated to *H_2CO (step 3), followed by desorption to form

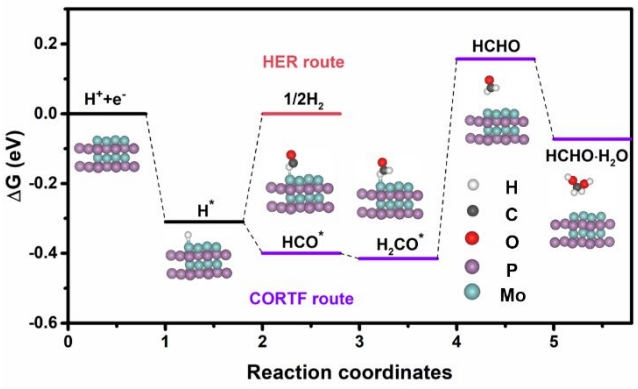

Figure 4. Gibbs free energy diagram of DFT-simulated CORTF and HER pathways at E=0 V.

HCHO (step 4) and by solvation to form dissolved HCHO (step 5). Thus the CORTF reaction pathway combines both galvanic and non-galvanic steps, which makes it subject to the influence of both electrochemical and thermal factors. The most energy demanding step for CORTF is found to be *HCHO desorption, which is likely the

rate-limiting step. Moreover, the result agrees with the reaction thermodynamics that direct CO reduction to gas phase HCHO has a positive ΔG value of 0.16 eV. The solvation effect due to HCHO dissolution in water turns the overall reaction into a spontaneous process (ΔG=-0.06 eV).

Spontaneous CO Hydrogenation to Formaldehyde in Full Cell Configuration

Based on the finding that the MoP can catalyze CORTF with high selectivity at E > 0 V, spontaneous CO hydrogenation to HCHO was demonstrated in a full cell configuration. **Figure 5a** and **Figure S21** show schematic and photograph of a simple H-type two-compartment cell set-up, which consists of carbon cloth-supported MoP as cathode, Pt wire as anode and aqueous KOH as electrolyte. An anion exchange membrane was employed between the two compartments that allows hydroxyl ion migration across the membrane and prevents crossover of gases. CO was fed to the cathode compartment where CORTF occurs leading to solvated HCHO formation (Eq. 4), and H_2 was simultaneously fed to the anode compartment where hydrogen oxidation reaction occurs (Eq. 5). **Figure 5b** shows the full cell testing results with different voltage loads. Interestingly even under zero cell voltage condition, HCHO was still produced at a rate of 6.1 mg/(g_{cat} h), indicating spontaneity characteristic of the reaction. Thus direct HCHO synthesis from CO hydrogenation can be realized without any energy input under ambient condition with a full electrochemical cell setup. A faster HCHO formation rate was yielded with a more negative cell voltage, which was in consistence with the observed potential dependency of the CORTF activity on MoP. It needs noted that the achieved HCHO formation rate under the full cell condition was lower than that under the half-cell condition, which was attributed to a considerable internal resistance of the anion exchange membrane and the simple cell setup without optimization. The durability of the full cell for HCHO production was evaluated at 0 V for 24 h (**Figure 5c**). HCHO was continuously produced under the testing condition as evidenced by its measured accumulated amount over reaction time. Less than 5 μA cm^{-2} decay in the current density was witnessed during the 24h test, indicating good cell durability property.

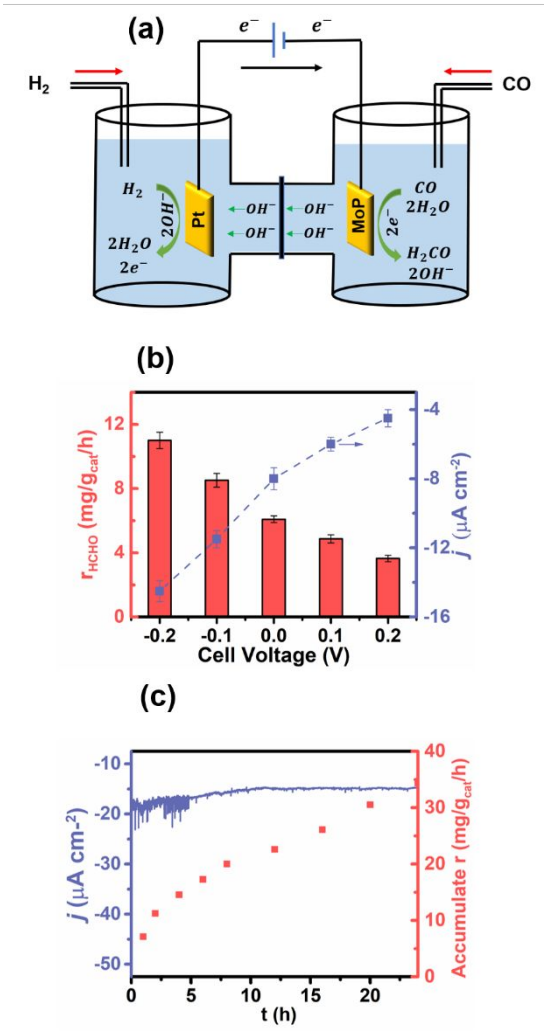

Figure 5. Spontaneous formaldehyde production demonstration in a full cell. (a) Graphic representation of the full-cell configuration. (b) Formaldehyde formation rate as function of cell voltage. (c) Cell durability test at 0 V cell voltage.

CONCLUSIONS

In summary, we report a new strategy for realizing direct CO reduction to formaldehyde (CORTF) under ambient condition by means of combining electrochemical and thermal approaches. For the first time formaldehyde was successfully produced at room temperature and ambient pressure in aqueous medium. The experimental results and DFT simulations suggest the reaction initiates by means of "sharing" the hydrogen underpotential deposition (HUPD) with HER, where H_{ad} is in situ electrocatalytically generated on MoP. This breaks down the scaling relationship restriction in thermal CO reduction catalysis, wherein H_2 dissociative adsorption to generate H_{ad} is strongly inhibited due to always stronger CO adsorption that poisons the catalyst. CO then reacts with H_{ad} following the thermal catalysis pathway that leads to formaldehyde formation. Up to 100% CORTF Faradaic efficiency was achieved by controlling a positive catalyst potential to inhibit HER. By tuning the electrochemical and thermal condition parameters, HCHO production rate as high as 31 mg/(g_{cat} h) was obtained, which was one order of magnitude higher than the previously reported thermal catalysis method (2~3 mg/(g_{cat} h)). More importantly, spontaneous CO hydrogenation to formaldehyde was realized by demonstrating the overall reaction in a full cell. Continuous formaldehyde production was observed by feeding CO and H_2 to the cathode and the anode without applying any cell voltage. The concept of hybridizing electrocatalysis and thermal catalysis for overcoming the thermodynamic barrier not only realizes successful direct spontaneous formaldehyde synthesis under ambient condition, but also is likely extendable to a wide range of thermodynamically and kinetically confined reactions.

Conflicts of interest

There are no conflicts to declare.

Acknowledgements

We acknowledge the financial support of this work by National Science Foundation (1665265).

The authors are grateful to Dr. Andrew Knoll at the National Polymer Innovation Center (NPIC) in University of Akron with the assistance of XPS. We are also grateful to Dr. Lingyan Li in National Center for Education and Research on Corrosion and Materials Performance (NCERAMP) at the University of Akron for the assistance of SEM analyses, and Mr. Thomas J. Quick in Geosciences Department at the University of Akron for the assistance of XRD. The HRTEM test was taken at the (cryo)TEM facility at the Liquid Crystal Institute, Kent State University, supported by the Ohio Research Scholars Program Research Cluster on Surfaces in Advanced Materials. The authors thank Dr. Min Gao for technical support with the TEM experiments.

References

(1) Acres, G. J. Recent advances in fuel cell technology and its applications. *J. Power Sources*. **2001**, 100, 60-66.
(2) Mahato, N.; Banerjee, A.; Gupta, A.; Omar, S.; Balani, K. Progress in material selection for solid oxide fuel cell technology: A review. *Prog. Mater. Sci*. **2015**, 72, 141-337.
(3) Schlapbach, L. Technology: Hydrogen-fuelled vehicles. *Nature*. **2009**, 460, 809.
(4) Sharaf, O. Z.; Orhan, M. F. An overview of fuel cell technology: Fundamentals and applications. *Renew. Sustain. Energy Rev*. **2014**, 32, 810-853.
(5) McWhorter, S.; Read, C.; Ordaz, G.; Stetson, N. Materials-based hydrogen storage: attributes for near-term, early market PEM fuel cells. Curr. Opin. *Solid. State. Mater. Sci*. **2011**, 15, 29-38.
(6) Demirci, U. B.; Miele, P. Chemical hydrogen storage: 'material' gravimetric capacity versus 'system'gravimetric capacity. *Energy Environ. Sci.* **2011**, 4, 3334-3341.
(7) Teichmann, D.; Arlt, W.; Wasserscheid, P.; Freymann, R. A future energy supply based on Liquid Organic Hydrogen Carriers (LOHC). *Energy Environ. Sci*. **2011**, 4, 2767-2773.
(8) Teichmann, D.; Arlt, W.; Wasserscheid, P. Liquid Organic Hydrogen Carriers as an efficient vector for the transport and storage of renewable energy. *Int. J. Hydrogen Energy*. **2012**, 37, 18118-18132.
(9) Eberle, U.; Felderhoff, M.; Schueth, F. Chemical and physical solutions for hydrogen storage. *Angew. Chem. Int. Ed*. **2009**, 48, 6608-6630.
(10) Onishi, N.; Laurenczy, G.; Beller, M.; Himeda, Y. Recent progress for reversible homogeneous catalytic hydrogen storage in formic acid and in methanol. *Coordin. Chem. Rev*. **2018**, 373, 317-332.
(11) Heim, L. E.; Konnerth, H.; Prechtl, M. H. Future perspectives for formaldehyde: pathways for reductive synthesis and energy storage. *Green Chem*. **2017**, 19, 2347-2355.
(12) Heim, L. E.; Schlörer, N. E.; Choi, J.-H.; Prechtl, M. H. Selective and mild hydrogen production using water and formaldehyde. *Nat. Comm.* **2014**, 5, 3621.
(13) Palo, D. R.; Dagle, R. A.; Holladay, J. D. Methanol steam reforming for hydrogen production. *Chem. Rev*. **2007**, 107, 3992-4021.
(14) Bi, Y.; Lu, G. Nano-Cu catalyze hydrogen production from formaldehyde solution at room temperature. *Int. J. Hydrogen Energy*. **2008**, 33, 2225-2232.
(15) Enthaler, S.; von Langermann, J.; Schmidt, T. Carbon dioxide and formic acid-the couple for environmental-friendly hydrogen storage? *Energy Environ. Sci*. **2010**, 3, 1207-1217.
(16) Brown, M.; Parkyns, N. Progress in the partial oxidation of methane to methanol and formaldehyde. *Catal. Today*. **1991**, 8, 305-335.
(17) Bahmanpour, A. M.; Hoadley, A.; Tanksale, A. Critical review and exergy analysis of formaldehyde production processes. *Rev. Chem. Eng*. **2014**, 30, 583-604.
(18) Tijm, P.; Waller, F.; Brown, D. Methanol technology developments for the new millennium. *Appl. Catal. A-Gen*. **2001**, 221, 275-282.
(19) Álvarez, A.; Bansode, A.; Urakawa, A.; Bavykina, A. V.; Wezendonk, T. A.; Makkee, M.; Gascon, J.; Kapteijn, F. Challenges in the greener production of formates/formic acid, methanol, and DME by heterogeneously catalyzed CO_2 hydrogenation processes. *Chem. Rev*. **2017**, 117, 9804-9838.
(20) Tang, X.; Bai, Y.; Duong, A.; Smith, M. T.; Li, L.; Zhang, L. Formaldehyde in China: production, consumption, exposure levels, and health effects. *Environ. Int.* **2009**, 35, 1210-1224.
(21) Gerberich, H. R.; Seaman, G. C.; Staff, U. b. Formaldehyde. *Kirk-Othmer Encyclopedia of Chemical Technology*. **2000**, 1-22.
(22) Bahmanpour, A. M.; Hoadley, A.; Tanksale, A. Formaldehyde production via hydrogenation of carbon monoxide in the aqueous phase. *Green Chem*. **2015**, 17, 3500-3507.
(23) Bahmanpour, A. M.; Hoadley, A.; Mushrif, S. H.; Tanksale, A. Hydrogenation of carbon monoxide into formaldehyde in liquid media. *ACS Sustain. Chem. Eng*. **2016**, 4, 3970-3977.
(24) Sun, G.; Zhao, Z.-J.; Mu, R.; Zha, S.; Li, L.; Chen, S.; Zang, K.; Luo, J.; Li, Z.; Purdy, S. C. Breaking the scaling relationship via thermally stable Pt/Cu single atom alloys for catalytic dehydrogenation. *Nat. Comm*. **2018**, 9, 4454.
(25) Fernández, E. M.; Moses, P. G.; Toftelund, A.; Hansen, H. A.; Martínez, J. I.; Abild-Pedersen, F.; Kleis, J.; Hinnemann, B.; Rossmeisl, J.; Bligaard, T. Scaling relationships for adsorption energies on transition metal oxide, sulfide, and nitride surfaces. *Angew. Chem. Int. Ed*. **2008**, 47, 4683-4686.
(26) Hong, X.; Chan, K.; Tsai, C.; Nørskov, J. K. How doped MoS_2 breaks transition-metal scaling relations for CO_2 electrochemical reduction. *ACS Catal*. **2016**, 6, 4428-4437.
(27) Feng, X.; Jiang, K.; Fan, S.; Kanan, M. W. A direct grain-boundary-activity correlation for CO electroreduction on Cu nanoparticles. *ACS Central Sci*. **2016**, 2, 169-174.
(28) Li, C. W.; Ciston, J.; Kanan, M. W. Electroreduction of carbon monoxide to liquid fuel on oxide-derived nanocrystalline copper. *Nature*. **2014**, 508, 504.
(29) Luc, W.; Fu, X.; Shi, J.; Lv, J.-J.; Jouny, M.; Ko, B. H.; Xu, Y.; Tu, Q.; Hu, X.; Wu, J. Two-dimensional copper nanosheets for electrochemical reduction of carbon monoxide to acetate. *Nat. Catal*. **2019**, 2, 423.
(30) Zhang, H.; Chang, X.; Chen, J. G.; Goddard, W. A.; Xu, B.; Cheng, M.-J.; Lu, Q. Computational and experimental demonstrations of one-pot tandem catalysis for electrochemical carbon dioxide reduction to methane. *Nat. Comm*. **2019**, 10, 3340.
(31) Ma, Z.; Porosoff, M. D. Development of tandem catalysts for CO_2 hydrogenation to olefins. *ACS Catal*. **2019**, 9, 2639-2656.
(32) Huang, J.; Mensi, M.; Oveisi, E.; Mantella, V.; Buonsanti, R. Structural Sensitivities in Bimetallic Catalysts for Electrochemical CO_2

Reduction Revealed by Ag–Cu Nanodimers. *J. Am. Chem. Soc*. **2019**, 141, 2490-2499.

(33) Hori, Y.; Murata, A.; Takahashi, R.; Suzuki, S. Electroreduction of carbon monoxide to methane and ethylene at a copper electrode in aqueous solutions at ambient temperature and pressure. *J. Am. Chem. Soc.* **1987**, 109, 5022-5023.

(34) Wang, X.; de Araújo, J. F.; Ju, W.; Bagger, A.; Schmies, H.; Kühl, S.; Rossmeisl, J.; Strasser, P. Mechanistic reaction pathways of enhanced ethylene yields during electroreduction of CO_2-CO co-feeds on Cu and Cu-tandem electrocatalysts. *Nat. Nanotechnol*. **2019**, 14, 1063-1070.

(35) Hori, Y.; Murata, A.; Takahashi, R.; Suzuki, S. Electrochemical reduction of carbon monoxide to hydrocarbons at various metal electrodes in aqueous solution. *Chem. Lett.* **1987**, 16, 1665-1668.

(36) Hansen, H.; Shi, C.; Lausche, A.; Peterson, A.; Nørskov, J. Bifunctional Alloys for the Electroreduction of CO_2 and CO. *Phys. Chem. Chem. Phys.* **2016**, 18, 9194-9201.

(37) Bertheussen, E.; Verdaguer-Casadevall, A.; Ravasio, D.; Montoya, J. H.; Trimarco, D. B.; Roy, C.; Meier, S.; Wendland, J.; Nørskov, J. K.; Stephens, I. E. Acetaldehyde as an intermediate in the electroreduction of carbon monoxide to ethanol on oxide-derived copper. *Angew. Chem. Int. Ed*. **2016**, 55, 1450-1454.

(38) Schouten, K. J. P.; Pérez Gallent, E.; Koper, M. T. Structure sensitivity of the electrochemical reduction of carbon monoxide on copper single crystals. *ACS Catal*. **2013**, 3, 1292-1295.

(39) Jouny, M.; Luc, W.; Jiao, F. High-rate electroreduction of carbon monoxide to multi-carbon products. *Nat. Catal*. **2018**, 1, 748.

(40) An, T.-Y.; Surendran, S.; Kim, H.; Choe, W.-S.; Kim, J. K.; Sim, U. A polydopamine-mediated biomimetic facile synthesis of molybdenum carbide-phosphide nanodots encapsulated in carbon shell for electrochemical hydrogen evolution reaction with long-term durability. *Compos. Part. B-Eng.* **2019**, 175, 107071.

(41) Duyar, M. S.; Tsai, C.; Snider, J. L.; Singh, J. A.; Gallo, A.; Yoo, J. S.; Medford, A. J.; Abild-Pedersen, F.; Studt, F.; Kibsgaard, J. A Highly Active Molybdenum Phosphide Catalyst for Methanol Synthesis from CO and CO_2. *Angew. Chem. Int. Ed*. **2018**, 130, 15265-15270.

(42) Wu, P.-w.; Chang, C.-c.; Chou, S.-s. Determination of formaldehyde in cosmetics by HPLC method and acetylacetone method. *J. Food Drug Anal*. **2003**, 11, 8-15.

(43) Giannozzi, P.; Baroni, S.; Bonini, N.; Calandra, M.; Car, R.; Cavazzoni, C.; Ceresoli, D.; Chiarotti, G. L.; Cococcioni, M.; Dabo, I. QUANTUM ESPRESSO: a modular and open-source software project for quantum simulations of materials. *J. Phys. Condens. Matter.* **2009**, 21, 395502.

(44) Dal Corso, A. Pseudopotentials periodic table: From H to Pu. *Comp. Mater. Sci*. **2014**, 95, 337-350.

(45) Xiao, P.; Sk, M. A.; Thia, L.; Ge, X.; Lim, R. J.; Wang, J.-Y.; Lim, K. H.; Wang, X. Molybdenum phosphide as an efficient electrocatalyst for the hydrogen evolution reaction. *Energy Environ. Sci.* **2014**, 7, 2624-2629.

(46) Zhou, Z.; Wei, L.; Wang, Y.; Karahan, H. E.; Chen, Z.; Lei, Y.; Chen, X.; Zhai, S.; Liao, X.; Chen, Y. Hydrogen evolution reaction activity of nickel phosphide is highly sensitive to electrolyte pH. *J. Mater. Chem. A.* **2017,** 5, 20390-20397.

(47) Wu, M.; Shen, P. K.; Wei, Z.; Song, S.; Nie, M. High activity PtPd-WC/C electrocatalyst for hydrogen evolution reaction. *J. Power Sources.* **2007,** 166, 310-316.

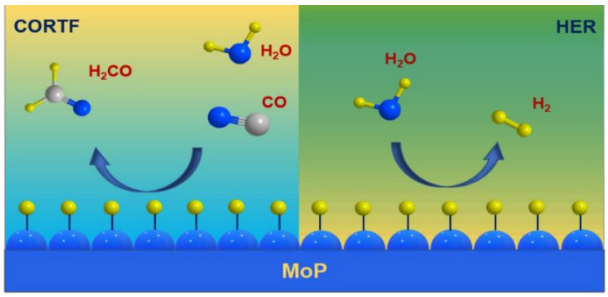

Highly selective formaldehyde production via CO electro-reduction utilizing hydrogen under-potential deposition under ambient condition.